Fractal aggregation in silica sols in basic tetraethoxysilane/ethanol/water solutions by small-angle neutron scattering

Tomchuk O.V.[1,2,*], *Bulavin L.A.*[2,3], *Pipich V.*[4], *Ryukhtin V.*[5], *Ivankov O.I.*[1,3,6], *Aksenov V.L.*[7,1], *Avdeev M.V.*[1]

[1] Frank Laboratory of Neutron Physics, Joint Institute for Nuclear Research, Dubna 141980, Russia

[2] Faculty of Physics, Taras Shevchenko National University of Kyiv, Kyiv 03022, Ukraine

[3] Institute for Safety Problems of Nuclear Power Plants, Chernobyl 07270, Ukraine

[4] Jülich Centre for Neutron Science at Heinz Maier-Leibnitz Zentrum, Garching 85747, Munich, Germany

[5] Neutron Physics Department, Nuclear Physics Institute, ASCR, v.v.i., Řež 25068, Czechia

[6] Moscow Institute of Physics and Technology, Dolgoprudny 141701, Russia

[7] National Research Centre "Kurchatov Institute", Moscow 123182, Russia

* *Corresponding author:* tomchuk@jinr.ru

Conventional small-angle neutron scattering (SANS) and ultrasmall-angle neutron scattering (USANS) are applied in the combined analysis of aggregated silica particles formed in basic tetraethoxysilane/ethanol/water solutions. The scattering is followed for different water/TEOS molar ratios to make a self-consistent description of fractal and size characteristics of the developed aggregates.

Introduction

A popular gel production technology is based on the so-called sol-gel technique, which consists of two principally different stages. First, sol formation is induced in a solution, then it is converted into a gel, a colloidal system consisting of a liquid dispersion medium enclosed in a flexible but sufficiently stable spatial network formed by the connected structural units of the solid phase [1,2]. This technique is used in the production of a wide range of industrial goods, from foods to adsorbents [3–5]. The well-proven sol-gel process employs the processes of controlled hydrolysis of alkoxides in aqueous or organic (often alcoholic) media followed by gelation as a result of an increase in the volume concentration of the solid phase or other changes in solutions (*e.g.*, pH variation, solvent replacement, *etc.*) [6].

The most common inorganic gel is silica gel obtained by polymerization of orthosilicic acid ($Si(OH)_4$) in aqueous solutions. Tetraethyl orthosilicate ($Si(OC_2H_5)_4$, TEOS) is often used as a precursor to initiate the growth of branched silicon-based structures [7–9]. The final gel organization, which greatly depends on the water content in the system as well as on the catalyst nature, is the result of the competitive effects of the hydrolysis and polycondensation reaction, which can be regulated by varying pH. Generally, silica gels grown in acidic solutions have a network consisting of linear polymeric-like agglomerates with a low density of cross bonds, while basic solutions give a network of highly branched clusters.

In the second case, the developed structures consisting of discrete colloidal particles (the size of which does not exceed several tens of nm) at certain concentrations are extensive networks formed throughout the liquid carrier via branched bonds. They have been studied by small-angle X-ray (SAXS) and neutron (SANS) scattering [10] for the last decades as objects with a fractal

scaling. The corresponding behavior of scattering curves is of a power-law type with the exponent directly related to the fractal dimension of the developed structures. The appearance of the primary fractal aggregation can be followed by SAXS/SANS starting from sols [11–13]. The recent application of the SANS contrast variation based on hydrogen/deuterium substitution in different components have clarified the inner structure of the basic structural units of the aggregates formed in basic conditions [14,15]. The scaling can vary in these systems in different correlation length ranges, which is mostly determined by the concentration of the initial components in the starting solutions and the water/TEOS molar ratio, *w*. Thus, when changing *w* in a wide interval of 1 – 10 at a fixed TEOS concentration one observes a monotonous decrease in the fractal dimension of the aggregates from 2 to 1 [11]. At the same time, the *w*-dependences for the structural parameters of the basic structural units including particle size and surface roughness are characterized by a critical behavior in the vicinity of $w = 2$ showing 'breaks' in corresponding functions. The fact that the growth processes at two structural levels are independent raises a question about the crossover between the mass and surface structural organizations.

For this purpose, in this work together with conventional small-angle neutron scattering (SANS) we have applied ultra-small-angle neutron scattering (USANS). The combination allows one to characterize materials in a significantly wider scale interval from nano- to micro-size levels. The small-angle scattering technique provides statistical information averaged over macroscopic volume, which can be related to the features of hydrolysis and aggregation mechanisms in the whole volume of final sols. If conventional SANS covers the level of nanoparticles and is partially sensitive to large (size above 100 nm) aggregates, the USANS technique specifically 'sees' aggregates in sols. This scale has not been studied before [11] because of resolution limitations in conventional SANS. Besides the reliable determination of the aggregate size, analysis is required to investigate in more detail the fractal structure of the aggregates in addition to their fractal dimensions estimated earlier [16–21]. Fractality is primarily associated with porosity and specific surface area [22], which determine the effectiveness of technological applications of silicate gels. For self-similar fractals, the aggregation number, N_a, and the fractal dimension, D, as well as the radius of gyration of the aggregates, R_a, and constituent particles, R_p, respectively, are related as:

$$N_a = k\left(R_a / R_p\right)^D . \qquad (1)$$

The prefactor, k, is a dimensionless constant of the order of unity. It is a local characteristic depending on the chosen center of the fractal associate. Its value is less if there are large empty areas within the aggregate, and *vice versa*. Fluctuations of k, depending on the position of the center in the system, are characterized by the parameter called lacunarity. Mandelbrot suggested [22] that the magnitude of the prefactor k is approximately inversely proportional to lacunarity, but this definition does not cover all cases. There are a number of methods proposed for calculating lacunarity, however, there is no general agreement regarding a strictly correct procedure [23,24]. Roughly, k can be associated with the porosity of the system, i.e. with the presence of large (compared to the size of the subunits of the fractal aggregate) pores [25]. The goal of this paper is determine all structural parameters provided by Eq. 1 for a complete description of fractal silica aggregates grown by basic hydrolysis in TEOS/ethanol/water ternary mixtures.

Experimental

Sols were prepared according to the procedure described in Refs. [11–15] by hydrolysis/polymerization of TEOS (10 wt.%) in aqueous-alcoholic solutions (pH ≈ 7.5) initiated by the addition of ammonium hydroxide to obtain the basic medium (pH increased to ≈ 10.5) so

that the H_2O/TEOS molar ratio was changed from 0.5 to 10 to cover the previously reported *w*-range. The samples were prepared seven days before the start of the experiment, with the exception of the series in which growth kinetics was monitored for 1–7 days (providing samples of different ages). To perform the external contrast variation procedure, solutions were prepared on the basis of the corresponding isotopic mixtures of H-ethanol and D-ethanol. For internal contrast variation, hydrolysis was initiated by light and heavy water, respectively. Sample preparation, storage and neutron scattering measurements were performed at 20°C.

To determine the structure of silicate sols under study, several series of SANS and USANS experiments were carried out. Conventional SANS was obtained on the YuMO time-of-flight diffractometer (IBR-2 pulsed reactor, FLNP JINR, Dubna, Russia); USANS experiments were performed on the KWS-3 high-resolution setup (FRM-II steady-state reactor, MLZ JCNS, Garching, Germany) and double-crystal high-resolution diffractometer MAUD (LVR15 steady-state reactor, CANAM infrastructure of NPI ASCR, Řež, Czech Republic).

At YuMO, SANS differential cross section per unit sample volume, $I(q)$, was obtained in a q-range of (0.08–4) nm^{-1}; neutron wavelength range (0.05–0.5) nm [26]. The scattering was recorded by two large-area ring-type ^{3}He detectors of isotropic scattering located at the sample-detector distances of 4.5 and 13 m, respectively. The absolute calibration of the scattered intensity was made using vanadium standards.

KWS-3 is a high-resolution small-angle diffractometer using a toroidal focusing mirror, which allows one to achieve a minimum momentum transfer at the level of 1×10^{-3} nm^{-1} [27]. The measurements at this instrument were made at a neutron wavelength of $\lambda = 1.28$ nm ($\Delta\lambda/\lambda = 0.2$). Sample-detector distances of 1 and 10 m covered the momentum transfer range of $q = (5\times10^{-3} – 1.5\times10^{-1})$ nm^{-1}. The scattered neutrons were detected with a 2D position-sensitive ^{6}Li-based detector (active area diameter of 8.7 cm with a spatial resolution of 0.36×0.39 mm). The obtained 2D patterns were azimuthally averaged and converted to the absolute scale by normalization to the incoherent scattering cross section of Plexiglas with taking into account the detector sensitivity.

USANS measurements using MAUD [28] were made at a neutron wavelength of 0.209 nm. Unlike conventional double-crystal diffractometers, the MAUD diffractometer is equipped with an elastically bent Si crystal analyzer, which allows the entire scattering pattern to be obtained on a 1D position-sensitive detector without rotation. The momentum transfer range was $q = (5\times10^{-3} – 1.2\times10^{-1})$ nm^{-1}.

In all experiments, sols were placed in flat 1-mm-thick quartz cells (Helma). The scattering by similar freshly prepared systems without the addition of ammonium hydroxide was subtracted as a background signal. To check the results of different calibration procedures, we obtained the scattering patterns for several samples on two instruments and the curves showed complete reproducibility in the overlapping q-ranges.

Results and discussion

The final structure of aggregated silica particles strongly depends on the water/TEOS molar ratio, but for the case under consideration (10% TEOS in alcohol-water solutions) the formation of colloidal particles always lasts about five days in ambient conditions, after which a period of relative structural stability is observed [11–13]. We confirmed this fact by comparatively short measurements of SANS curves for the samples of identical composition ($w = 2$), but of different ages. In Fig. 1 it is clearly seen that on the sixth day, the exponential growth of sol nanoparticles significantly slows down and some saturation occurs. This makes it possible to carry out a series of SANS experiments that are more extended in time (up to several days).

In the literature, including our previous results on neutron scattering [14,29], it was concluded that sol particles are close in structure to amorphous silicon dioxide. It is important that recent experiments on SANS contrast variation excluded any significant presence of hydroxyl groups inside colloidal particles [14,15], which was discussed [12,13] at the early stages of structural research of the given systems within the framework of the model of poisoned bonds. Nevertheless, a certain amount of hydroxyl groups can be present on the particle surface in amounts undetectable by SANS. They are involved in the stabilization of the particles, and, when the solution is concentrated, participate in the formation of a gel network at the second stage of the sol-gel process.

Contrast variation is a strong advantage of neutron scattering methods. In the course of such type of experiments, one can track changes in the scattering curves after isotopic substitution (most often hydrogen for deuterium) in the solution only slightly affecting the chemical properties of the components. Thus, in our previous works [14,15], the hydrolysis of TEOS was carried out by both light and heavy water. The solvent scattering length density (SLD) in this case is practically unchanged due to rather small volume fraction of water in the whole system. Any noticeable presence of hydroxyl groups in the composition of the dispersed phase would lead to a difference in the scattering curves. Yet, conventional SANS setups do not reveal any difference. Hence, it was concluded that the vast majority of hydrolyzed $\equiv Si-O-H(D)$ bonds participate in the polycondensation reaction with the formation of $\equiv Si-O-Si\equiv$, since the sol structure is identical for the TEOS/C_2H_6O/H_2O and TEOS/C_2H_6O/D_2O systems at a scale of $L < 90$ nm. The latter limit was estimated from the relation between direct and reciprocal Fourier space, $L_{max} \approx 2\pi/q_{min}$. In the current research, using USANS, the size scale have been extended to $L_{max} \approx 900$ nm. Again, the scattering data (Fig. 2) confirm the previous conclusions, since no isotope effect is observed at the submicron scale either. Thus, the internal contrast variation (variation in the scattering density of the dispersed phase) indicates that in the case of the basic synthesis no hydroxyl groups remain in the composition of the aggregates.

During the external contrast variation (SLD of the dispersion medium is changed), one can determine the average scattering length density of dispersed particles. Another potential structural difference in the products of the TEOS hydrolysis is that there are “immured” ethyl groups $\equiv Si-O-C_2H_5$ that do not have time to hydrolyze, since quite rapid condensation reaction limits the access of water molecules from the solvent [14]. To clarify this point, first, the Guinier approximation was tested for the intensity at the smallest scattering vectors, $qR_a \le 1$:

$$I(q) = G_a \exp\left(-q^2 R_a^2/3\right), \qquad (2)$$

Here, G_a is the forward scattered intensity, which has a quadratic dependence on contrast – the difference in the scattering length densities of the two phases:

$$G_a \sim \left(\bar{\rho} - \rho_S\right)^2 R_a^D . \qquad (3)$$

It should be noted that for the basic structural units of the aggregates in the vicinity of $qR_p \le 1$, the scattered intensity follows the law similar to equation (2), with the parameters G_p and R_p corresponding to the particle level. The average particle gyration radius obtained was (13.7 ± 0.3) nm. By extrapolating dependence (3) to minima for both levels (Fig.2*b*), the so-called match points, one obtains the average SLD of colloidal particles and aggregates, respectively. Experimentally, this is achieved by measuring samples with different volume contents of deuterated ethanol, η, that determines solvent SLD as $\rho_{solv} = \eta\rho_D + (1 - \eta)\,\rho_H$, where $\rho_D = 6.098\times10^{10}$ cm^{-2} and $\rho_H = -0.345\times10^{10}$ cm^{-2} are the scattering length density of the deuterated and nondeuterated ethanol, respectively.

Our previous SANS results at the scale of < 90 nm gave a value close (within 5%) to that for amorphous silicon dioxide. Here, we repeated this experiment, expanding the *q*-range towards ultra-small values. In this case, we were able to show that the analysis of the Guinier regions corresponding to both aggregates and sol particles gives almost the same match point. It is only 4.3% higher than the tabulated value for SLD of silicon dioxide. It is important to note that the presence of "immured" ethyl groups, on the contrary, would lower the average particle SLD, since they contain hydrogen with a negative scattering length [10]. Thus, SANS analysis of the structure of silicate sols obtained from hydrolyzed TEOS confirms that they consist of pure SiO_2.

The observed aggregation corresponding to the ultra-small *q*-range exhibits pronounced fractal properties. The scattering curve is described by a power law with an exponent close to 2. It lies in the interval of (1–3) (see Fig. 3*a*) and, thus, equals to the mass fractal dimension, *D* [30]. The previous experiments at conventional SANS setups did not resolve the size of these aggregates. The dependences of the Guinier parameters on the water/TEOS molar ratio are presented in Fig. 3*b*. Both dependencies, $G(w)$ and $R(w)$ monotonously decrease with increasing *w* following power laws, which is proved by linear approximations in the double logarithmic plots. The ratio of the corresponding power-law exponents is about 2.1, which is close to the fractal dimension of the aggregates ≈ 2, and the ratio G_a / R_a^D is close to a constant (shown in the inset to Fig. 3*b*) in full agreement with the scaling $G_a \sim R_a^D$ (Eq. 3) following from the theory of scattering by fractals [31]. It also proves full accessibility of the solvent to the surface of basic units; closed pores in the structure of the aggregates are excluded, since they would strongly affect the relations discussed.

The self-consistent description of the fractal structure of the aggregates which takes into account the cut-off effects with respect to the aggregate size, makes it possible to estimate the *k*-parameter in Eq. 1. Assuming a quasi-monodisperse size distribution, the aggregation number can be determined from SANS as:

$$N_a \approx \langle N^2 \rangle / \langle N \rangle = G_a / G_p \quad . \quad (4)$$

With almost constant G_p and monotonically decreasing G_a, the aggregation number drops by about one order (from ≈ 20 to ≈ 2) when *w* increases from 0.5 to 10 (Fig. 4), which fully correlates with a decrease in the aggregate size, R_a. Combining (1), (2) and (4) one obtains for the fractal prefactor, *k*:

$$k = \frac{G_a}{G_p} \left(\frac{R_p}{R_a} \right)^D . \quad (5)$$

Our data indicate that this parameter remains constant for different molar ratios of water to TEOS (see the inset in Fig. 4). The exception is the case of maximally achieved *w*, which is explained by a significant error in determining the Guinier parameters of the aggregates at small aggregation numbers. The fractal prefactor (determined by the porosity dependent lacunarity) is a characteristic of the entire class of objects obtained by the base-catalyzed hydrolysis of TEOS and further polycondensation of orthosilicic acid. This can be an important factor for developing production processes using the sol-gel method regarding both thin-film coatings and bulk porous materials.

The reproducibility of the results for the ultra-small *q*-region was additionally verified using USANS diffractometers based on different principles (Fig. 5). The corresponding curves obtained are in agreement; the general tendency for the SANS curves to decrease in their initial parts together with a slight increase at large *q*-values is undoubtedly traced. In the *q*-interval overlapping with the conventional SANS, the USANS curves repeat those from Ref. 11.

Conclusions

To summarize, the joint application of the conventional SANS and USANS methods made it possible to describe fractal aggregation in basic tetraethoxysilane/ethanol/water solutions in terms of a self-consistent model covering the combined size-range of nano- and submicron-levels. The extended analysis of the fractal structure allowed us to conclude that the effective measure of cluster porosity (fractal prefactor) for silica aggregates is constant for the sols obtained by hydrolyzed tetraethoxysilane regardless of the water/TEOS molar ratio. At the same time, an increase in this ratio leads to a significant decrease in the size of aggregates down to trimers and dimers for the largest value covered in the experiments. The experiments were done for the systems with the same pH required to start the initiation of hydrolysis and aggregate growth. The pH-effect on the whole process and final fractal structure of aggregates in combination with the variation of the TEOS concentration is the subject of further investigations.

Acknowledgments

This study was supported by the Russian Science Foundation (project no. 18-72-00099). The measurements at the Nuclear Physics Institute of the Academy of Sciences of the Czech Republic (Řež, Czech Republic) were performed using the infrastructure of the Center of Accelerators and Nuclear Analytical Methods (CANAM) with the support of the Ministry of Education, Youth and Sports (MEYS, MŠMT in Czech Republic) (project no. LM2011019). The measurements based on the infrastructure of MLZ and FLNP JINR are also gratefully acknowledged.

Research Highlights:

♦ Fractal structure of the sols obtained by hydrolyzed tetraethoxysilane was investigated

♦ Increase in the water/TEOS molar ratio leads to a significant decrease in the aggregate size

♦ Porosity of silica aggregates is constant regardless of this ratio

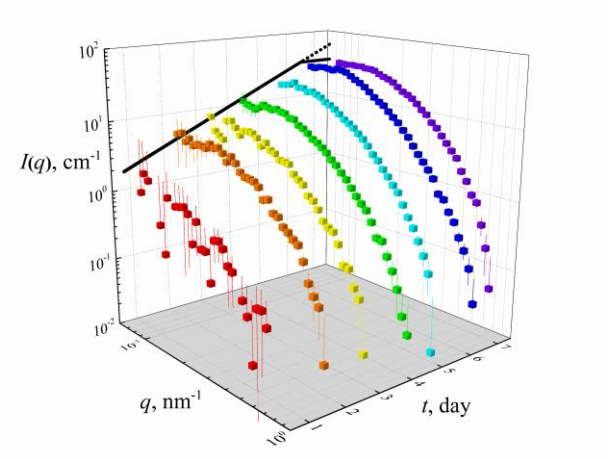

Fig. 1. Increase in SANS intensity corresponding to the growth of aggregates in the solutions under study during the first days after the initiation of the sol-gel process.

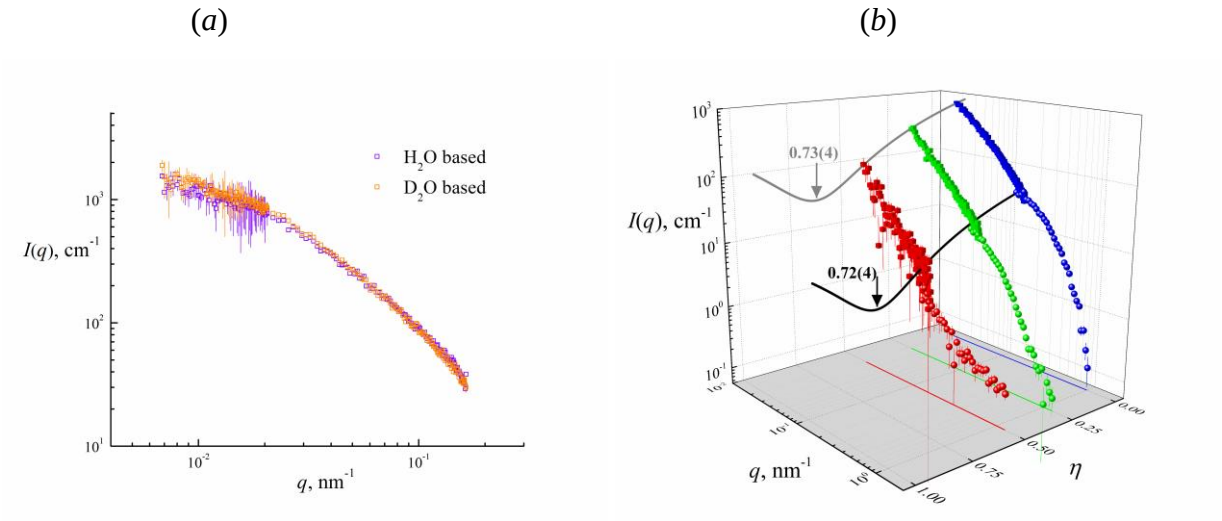

Fig. 2. SANS curve obtained in the experiments on internal (*a*) and external (*b*) contrast variation in silica sols with $w = 2$. In the second case, extrapolating quadratic dependences of scattered intensity on the contrast are shown for the levels of aggregates (gray line) and particles (black line), respectively; corresponding match-points (shown by arrows) are given in terms of D-ethanol volume fraction.

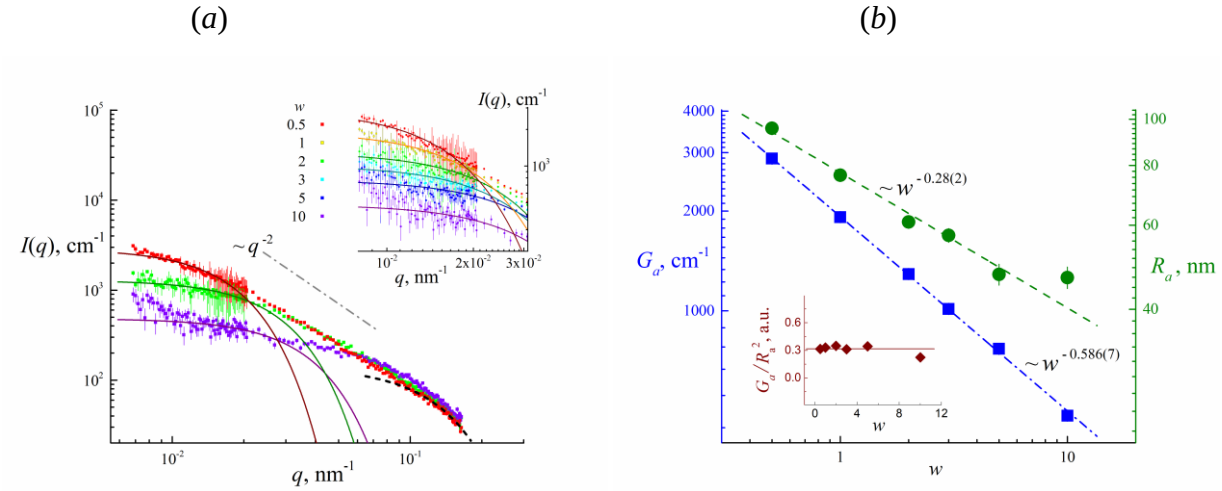

Fig. 3. (*a*) Experimental (points) SANS curves for different *w*-values with the Guinier approximation (lines); (*b*) Parameters of the Guinier approximation as a function of water/TEOS ratio. The lines show the corresponding scaling laws. The inset displays the *w*-dependence of the experimentally found ratio G_a / R_a^2 approximated with a constant.

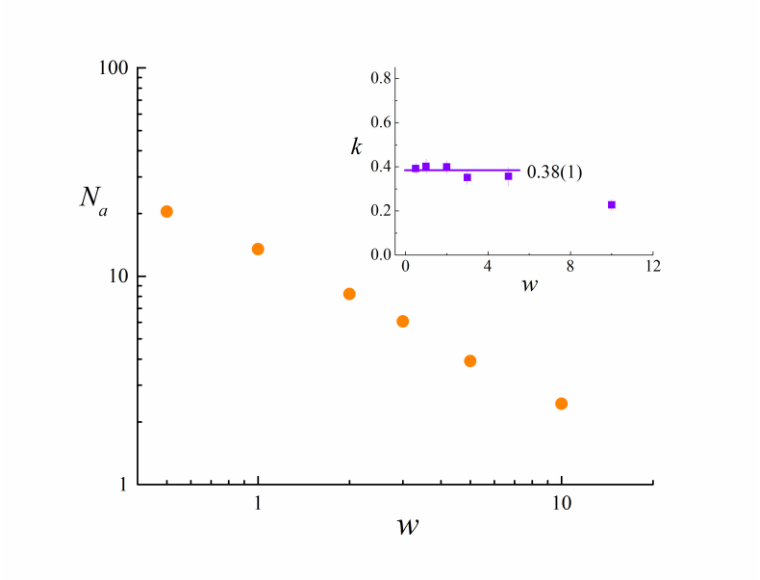

Fig. 4. Aggregation number of silica particles in the studied sols *vs.* water/TEOS molar ratio. In the inset, the *w*-dependence of the fractal prefactor is given with the indication of the average value.

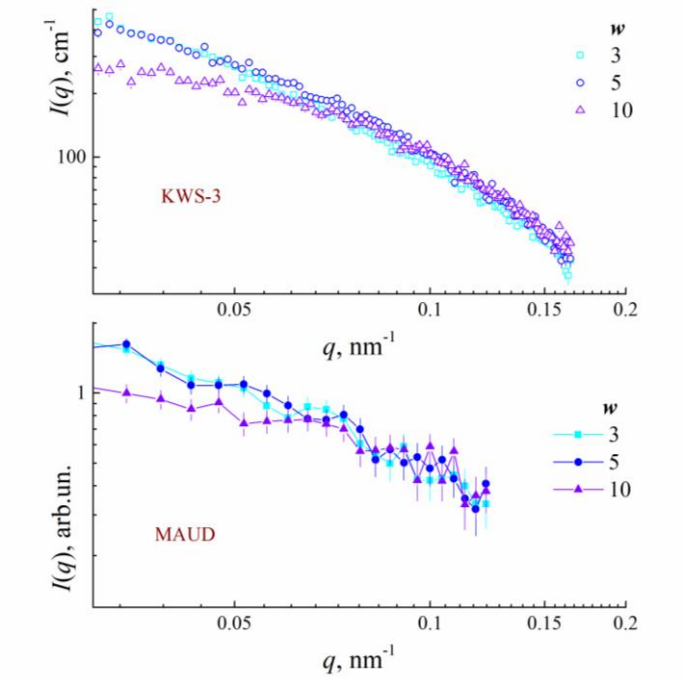

Fig. 5. Comparison of the experimental USANS curves for silica sols obtained at different setups (KWS-3@MLZ and MAUD@NPI ASCR). All samples are prepared by the same procedure as described in the Experimental section.

References

1. L.L. Hench, J.K. West, The sol-gel process, Chem. Rev. 90 (1990) 33–72; https://doi.org/10.1021/cr00099a003

2. S. Panyukov, Y. Rabin, Statistical physics of polymer gels, Phys. Rep. 269 (1996) 1–131; https://doi.org/10.1016/0370-1573(95)00068-2

3. S. Esposito, "Traditional" sol-gel chemistry as a powerful tool for the preparation of supported metal and metal oxide catalysts, Materials 12 (2019) 668; https://doi.org/10.3390/ma12040668

4. K. Pal, I. Banerjee (eds.), Polymeric gels: Characterization, properties and biomedical applications, Woodhead Publishing (2018) 568pp.; https://doi.org/10.1016/C2016-0-04092-5

5. S. Banerjee, S. Bhattacharya, Food gels: Gelling process and new applications, Crit. Rev. Food Sci. Nutr. 52 (2012) 334–346; https://doi.org/10.1080/10408398.2010.500234

6. C.J. Brinker, G.W. Scherer, Sol → gel → glass: I. Gelation and gel structure, J. Non-Cryst. Solids, 70 (1985) 301–322; https://doi.org/10.1016/0022-3093(85)90103-6

7. R.K. Iler, The chemistry of silica: Solubility, polymerization, colloid and surface properties, and biochemistry, Wiley: New York (1979) 896pp.; ISBN: 978-0-471-02404-0

8. A.V. Rao, S.D. Bhagat, Synthesis and physical properties of TEOS-based silica aerogels prepared by two step (acid–base) sol–gel process, Solid State Sci. 6 (2004) 945–952; https://doi.org/10.1016/j.solidstatesciences.2004.04.010

9. E.D.E.R. Hyde, A. Seyfaee, F. Neville, R. Moreno-Atanasio, Colloidal silica particle synthesis and future industrial manufacturing pathways: A review, Ind. Eng. Chem. Res. 55 (2016) 8891–8913; https://doi.org/10.1021/acs.iecr.6b01839

10. H. Brumberger (ed.), Modern aspects of small-angle scattering, Kluwer Academic Publishers: Dordrecht (1995) 463 pp.; https://doi.org/10.1007/978-94-015-8457-9

11. M.V. Avdeev, V.L. Aksenov, J. Kohlbrecher, L. Rosta, SANS study of colloidal aggregates of silicon tetraethoxide in basic ethanol/water solutions, Physica B 350 (2004) e905–e908; https://doi.org/10.1016/j.physb.2004.03.234

12. D.W. Schaefer, K.D. Keefer, Fractal geometry of silica condensation polymers, Phys. Rev. Lett. 53 (1984) 1383–1386; https://doi.org/10.1103/PhysRevLett.53.2457

13. K.D. Keefer, D.W. Schaefer, Growth of fractally rough colloids, Phys. Rev. Lett. 56 (1986) 2376–2379; https://doi.org/10.1103/PhysRevLett.56.2199

14. O.V. Tomchuk, M.V. Avdeev, L.A. Bulavin, V.V. Ryukhtin, O.I. Ivankov, V.L. Aksenov, A.V. Nagornyi, Study of tetraethoxysilane clusters in basic ethanol/water solutions by SANS contrast variation, Romanian J. Phys. 63 (2018) 906; http://www.nipne.ro/rjp/2018_63_7-8/RomJPhys.63.906.pdf

15. O.V. Tomchuk, M.V. Avdeev, O.I. Ivankov, L.A. Bulavin, V.L. Aksenov, Features of colloidal aggregation in tetraethoxysilane-water-ethanol ternary mixtures by small-angle neutron scattering, J. Surf. Invest. 13 (2019) 1122–1125; https://doi.org/10.1134/S1027451019060545

16. K. Yoshida, T. Zenin, A. Fujiyoshi, Y. Sanada, T. Yamaguchi, K. Murata, S. Takata, K. Hiroi, T. Takekiyo, Y. Yoshimura, The effect of alkyl ammonium ionic liquids on thermal denaturation aggregation of β-lactoglobulin, J. Mol. Liq. 293, (2019) 111477; https://doi.org/10.1016/j.molliq.2019.111477

17. R.D. Selvakumar, J. Wu, A comprehensive model for effective density of nanofluids based on particle clustering and interfacial layer formation, J. Mol. Liq. 292 (2019) 111415; https://doi.org/10.1016/j.molliq.2019.111415

18. A.V. Chalyi, Surface tension in bulk and bounded liquids, J. Mol. Liq. 288 (2019) 110873; https://doi.org/10.1016/j.molliq.2019.04.150

19. E.G. Iashina, M.V. Filatov, R.A. Pantina, E.Yu. Varfolomeeva, W.G. Bouwman, C.P. Duif, D. Honecker, V. Pipich, S.V. Grigoriev, Small-angle neutron scattering (SANS) and spinecho SANS measurements reveal the logarithmic fractal structure of the large-scale chromatin organization in HeLa nuclei, J. Appl. Cryst. 52 (2019) 844–853; https://doi.org/10.1107/S160057671900921X

20. J. Timmons, G. Falzone, M. Balonis, M. Bauchy, G. Sant, Anomalous variations in the viscous activation energy of suspensions induced by fractal structuring, J. Colloid Interface Sci. 530 (2018) 603–609; https://doi.org/10.1016/j.jcis.2018.07.008

21. T.V. Nagorna, M.O. Kuzmenko, O.A. Kyzyma, D. Chudoba, A.V. Nagornyi, T.V. Tropin, V.M. Garamus, M. Jazdzewska, L.A. Bulavin, Structural reorganization of fullerene C_{70} in N-methyl-2-pyrrolidone/toluene mixtures, J. Mol. Liq. 272 (2018) 948–952; https://doi.org/10.1016/j.molliq.2018.10.110

22. B.B. Mandelbrot, The fractal geometry of nature, W.H. Freeman: New York (1983) 460pp.; ISBN 0-7167-1186-9

23. C. Allain, M. Cloitre, Characterizing the lacunarity of random and deterministic fractal sets, Phys. Rev. A 44 (1991) 3552–3558; https://doi.org/10.1103/PhysRevA.44.3552

24. T.G. Smith Jr., G.D. Lange, W.B. Marks, Fractal methods and results in cellular morphology – dimensions, lacunarity and multifractals, J. Neurosci. Methods 69 (1996) 123–136; https://doi.org/10.1016/S0165-0270(96)00080-5

25. O. Agboola, M.S. Onyango, P. Popoola, O.A. Oyewo, Fractal geometry and porosity, in "Fractal Analysis" ed. by F. Brambila, 249–266; https://doi.org/10.5772/intechopen.68201

26. A.I. Kuklin, A.V. Rogachev, D.V. Soloviov, O.I. Ivankov, Y.S. Kovalev, P.K. Utrobin, S.A. Kutuzov, A.G. Soloviev, M.I. Rulev, V.I. Gordeliy, Neutronographic investigations of supramolecular structures on upgraded small-angle spectrometer YuMO, J. Phys.: Conf. Ser. 848 (2017) 012010; https://doi.org/10.1088/1742-6596/848/1/012010

27. Heinz Maier-Leibnitz Zentrum et al., KWS-3: Very small angle scattering diffractometer with focusing mirror, J. Large-Scale Res. Facil. 1 (2015) A31; https://doi.org/10.17815/jlsrf-1-28

28. P. Strunz, J. Šaroun, P. Mikula, P. Lukáš, F. Eichhorn, Double-bent-crystal small-angle neutron scattering setting and its applications, J. Appl. Cryst. 30 (1997) 844–848; https://doi.org/10.1107/S0021889897001271

29. V.M. Masalov, N.S. Sukhinina, G.A. Emel'chenko, Colloidal particles of silicon dioxide for the formation of opal-like structures, Phys. Solid State 53 (2011) 1135–1139; https://doi.org/10.1134/S1063783411060229

30. P.W. Schmidt, Small-angle scattering studies of disordered, porous and fractal systems, J. Appl. Cryst. 24 (1991) 414–435; https://doi.org/10.1107/S0021889891003400

31. J. Teixeira, Small-angle scattering by fractal systems, J Appl. Cryst. 21 (1988) 781–785; https://doi.org/10.1107/S0021889888000263